robotics

MDPI

Article

Stretchable and Compliant Sensing of Strain, Pressure and Vibration of Soft Deformable Structures

Darren Zi Hian Yeo [1,†], Catherine Jiayi Cai [1,2,†], Po-Yen Chen [3,*] and Hongliang Ren [1,4,*]

1 Department of Biomedical Engineering, National University of Singapore, Singapore 117575, Singapore
2 Singapore Institute of Manufacturing Technology, Singapore 138634, Singapore
3 Department of Chemical and Biomolecular Engineering, University of Maryland, College Park, MD 20742-2111, USA
4 Department of Electronic Engineering, Faculty of Engineering, The Chinese University of Hong Kong, Hong Kong 999077, China
* Correspondence: checp@umd.edu (P.-Y.C.); hlren@ieee.org (H.R.)
† These authors contributed equally to this work.

Abstract: Soft robotic and medical devices will greatly benefit from stretchable and compliant pressure sensors that can detect deformation and contact forces for control and task safety. In addition to traditional 2D buckling via planar substrates, 3D buckling via curved substrates has emerged as an alternative approach to generate tunable and highly convoluted hierarchical wrinkle morphologies. Such wrinkles may provide advantages in pressure sensing, such as increased sensitivity, ultra-stretchability, and detecting changing curvatures. In this work, we fabricated stretchable sensors using wrinkled MXene electrodes obtained from 3D buckling. We then characterized the sensors' performance in detecting strain, pressure, and vibrations. The fabricated wrinkled MXene electrode exhibited high stretchability of up to 250% and has a strain sensitivity of 0.1 between 0 and 80%. The fabricated bilayer MXene pressure sensor exhibited a pressure sensitivity of 0.935 kPa^{-1} and 0.188 kPa^{-1} at the lower (<0.25 kPa) and higher-pressure regimes (0.25 kPa–2.0 kPa), respectively. The recovery and response timing of the wrinkled MXene pressure sensor was found to be 250 ms and 400 ms, respectively. The sensor was also capable of detecting changing curvatures upon mounting onto an inflating balloon.

Keywords: MXene; vibration frequency response; strain sensing; pressure sensing

check for updates

Citation: Yeo, D.Z.H.; Cai, C.J.; Chen, P.-Y.; Ren, H. Stretchable and Compliant Sensing of Strain, Pressure and Vibration of Soft Deformable Structures. *Robotics* **2022**, *11*, 146. https://doi.org/10.3390/robotics11060146

Academic Editor: Kaspar Althoefer

Received: 17 October 2022
Accepted: 1 December 2022
Published: 6 December 2022

1. Introduction

In biomedical applications, it is desirable for soft robotic and medical devices to possess self-sensing capabilities for control and task safety [1,2]. These devices will greatly benefit from sensors that can estimate the device's shape as they undergo deformation and the contact locations and forces that the devices experience as they interact with the surrounding tissue [3,4]. Among the various transduction principles available, piezoresistive strain and pressure sensors are widely employed due to their simple working principle, cost-effective fabrication, and high sensitivity [5]. To accommodate and sustain the deformation of the soft devices without hindering their medical functions and abilities [6,7], these sensors need to be conformable, flexible, stretchable and compliant. One popular approach to fabricating stretchable electronics is buckling [2,8–11], where a conducting film is first deposited on a pre-strained elastomeric substrate. When the substrate undergoes relaxation, the pre-strain is released, and the formation of sinusoidal wavy patterns is induced onto the conducting film. These wavy patterns appear as wrinkles or buckles.

Traditional buckling approaches depend on the relaxation of pre-stretched planar elastomer substrates to create out-of-plane wrinkles [12–16]. Recently, various research groups have touted the benefits of using curved elastomeric substrates to create highly

folded patterns capable of dynamic tunability with hierarchical microstructures. In contrast to planar substrates that result in two-dimensional (2D) buckling, curved substrates enable three-dimensional (3D) buckling that is observed to generate multiscale and highly convoluted wrinkle morphologies [17,18]. The morphology of these created hierarchical wrinkles can be tuned by varying the shape and shrinking steps of the underlying curved elastomeric substrate [19]. For example, spherical surfaces result in wrinkle topographies that appear isotropic in every radial direction, while cylindrical surfaces result in more hierarchical and oriented wrinkle topologies [19].

The advantages of creating wrinkles via 3D buckling have been demonstrated in piezoresistive strain sensing, where the as-fabricated stretchable strain sensors demonstrated high sensitivity, high uni-directional stretchability, and ultrahigh areal stretchability [19]. However, to our knowledge, the advantages and applications of wrinkles created from 3D buckling have yet to be explored in pressure sensing. Stretchable and sensitive pressure sensors are often desirable in soft medical devices to detect contact forces for control and to reduce potential damage to the surrounding tissue [1,3]. To address this gap in the literature, we aim to fabricate and characterize the performance of stretchable wrinkled pressure sensors fabricated from 3D buckling.

2. Materials and Methods

The material chosen for the fabrication of piezoresistive sensors directly impacts the resulting mechanical compliance and electrical performance [8]. In this work, we chose to fabricate conductive electrodes using MXene, due to its inherent conductive properties and ease of preparation and application. MXene is a compound of transition metal carbide and nitride with the general formula $M_{n+1}X_nTx$, where M denotes transition metal, X denotes carbon and/or nitrogen, and T_x represents surface functional groups (surface termination groups such as O, OH and/or F) [20,21]. It also boasts a large specific surface area due to wrinkled laminated nanocrystals. MXene has been used in piezoresistive sensors and can transduce external pressure into a resistance signal. MXene-derivative piezoresistive sensors often exhibit resistance changes in response to deformation in geometry [21,22].

We obtained Ti_3AlC_2 MAX crystals from Xincailiao and etched them in situ with hydrofluoric acids (HF), according to the process mentioned in Ref. [23], to obtain Ti_3AlC_2 MXene ink (Figure 1c), which can be coated on substrates to form MXene thin films. As MXene films by themselves are not inherently stretchable, we employed 3D buckling to create hierarchical wrinkles on the films by using a balloon as a pre-stretched substrate, such as those mentioned in [17–19,24]. These wrinkles can be unfolded, allowing the films to stretch and flex [9].

We first inflated a long latex balloon to a controlled dimension and then brush-coated the surface of the inflated balloon with MXene ink of a suitable concentration (Figure 1a). When the MXene ink has air-dried to form a MXene film, we fully deflated the balloon circumferentially and longitudinally in one step, resembling a biaxial compression. The wrinkled MXene film can then be used as stretchable electrodes to fabricate strain and pressure sensors. The thickness of the resulting wrinkled MXene film will depend on the concentration of the MXene ink used. In general, using a higher concentration of MXene ink will give rise to a thicker wrinkled MXene film in a given coated area [8]. In this work, we used 400 μL of MXene ink of a concentration of 18 mg/mL on a painted area of 75 mm by 45 mm. This gave rise to a wrinkled MXene film (size 20 mm by 12 mm) of around 26 μm in thickness, as estimated from cross-sectional SEM. We then fabricated a piezoresistive strain sensor using a single layer of MXene electrode by attaching the MXene-balloon composite onto a VHB tape to confer additional mechanical stability to the sensor.

A bilayer piezoresistive pressure sensor was fabricated by attaching two MXene electrodes together (with the MXene film facing each other), using double-sided tape as the spacer (Figure 1b). This symmetrical sandwich structure in which the sensing layers are separated with a spacer is commonly employed as piezoresistive pressure sensors in literature [11,25,26].

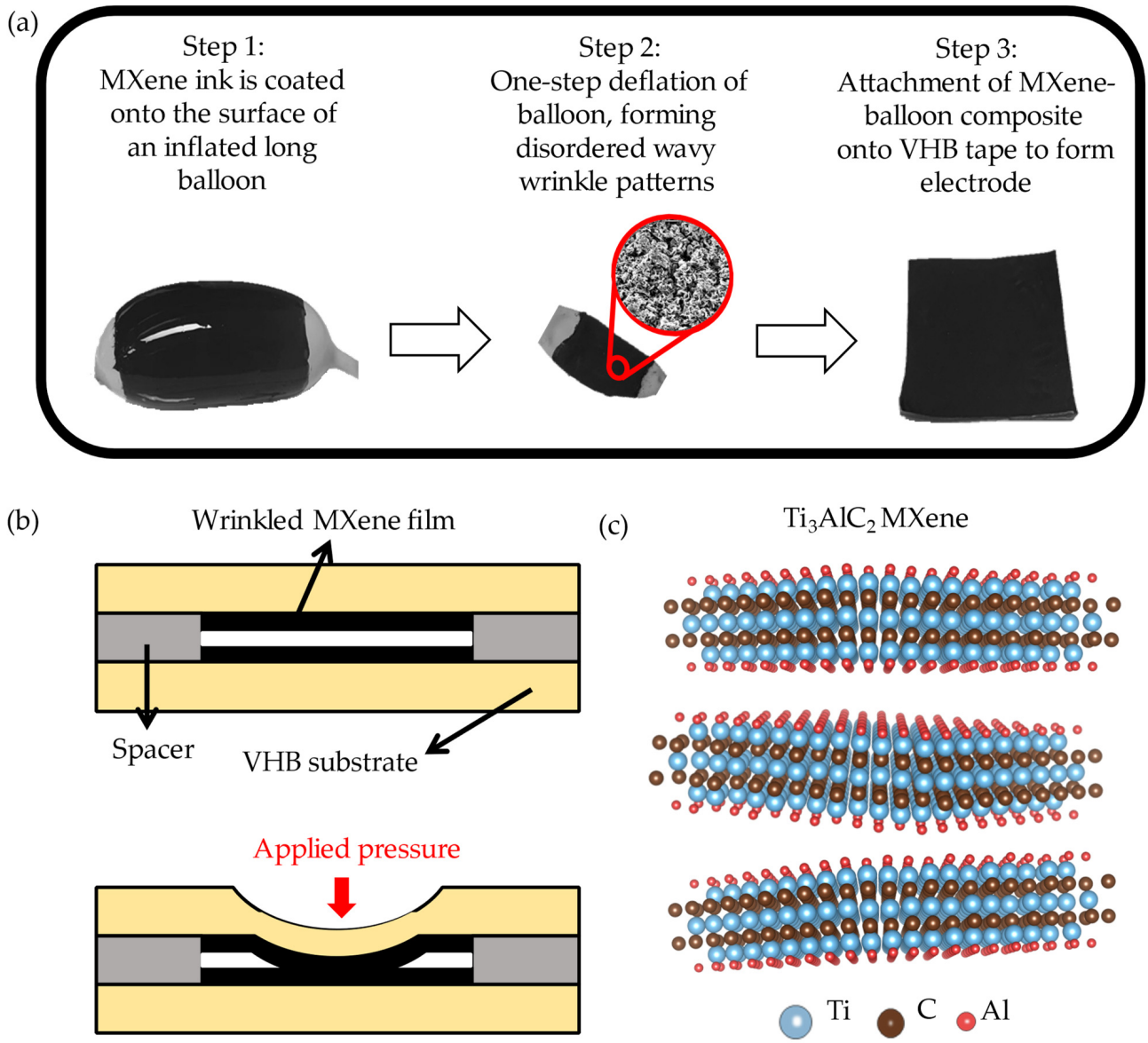

Figure 1. (**a**) Fabrication of wrinkled MXene electrode through 3D buckling. The as-wrinkled film can be used as a piezoresistive strain sensor. (**b**) A bilayer piezoresistive pressure sensor was fabricated by attaching two MXene electrodes together with a double-sided tape, which also functions as spacers. (**c**) Chemical architecture of Ti_3AlC_2 MXene.

We characterized the sensors' strain and pressure performances to ascertain their potential as sensors for soft robotics and medical devices. The resistance of the sensor was calculated by measuring the voltage drop across the sensor, through an Arduino UNO R3 microcontroller setup. Crocodile clips were attached to the copper tapes which were used as external connections (Figure 2a). PuTTy software was used to collect the numerical data from the microcontroller. The Arduino setup compares the resistance of the sensor (R_u) against that of a known resistor (R_1) under a constant supply of 5 V voltage (V_{in}) across the sensor at every 1 ms. The unknown resistance, R_u is then calculated through the equation: $R_u = R_1 * \left(\frac{V_{in}}{V_{out}} - 1\right)$, where V_{out} is the voltage output from the sensor electrodes to the Arduino controller. In this setup, we chose R_1 to be of a value close to that of the initial sensor's resistance. The results of the sensors' performances can be found in the following section.

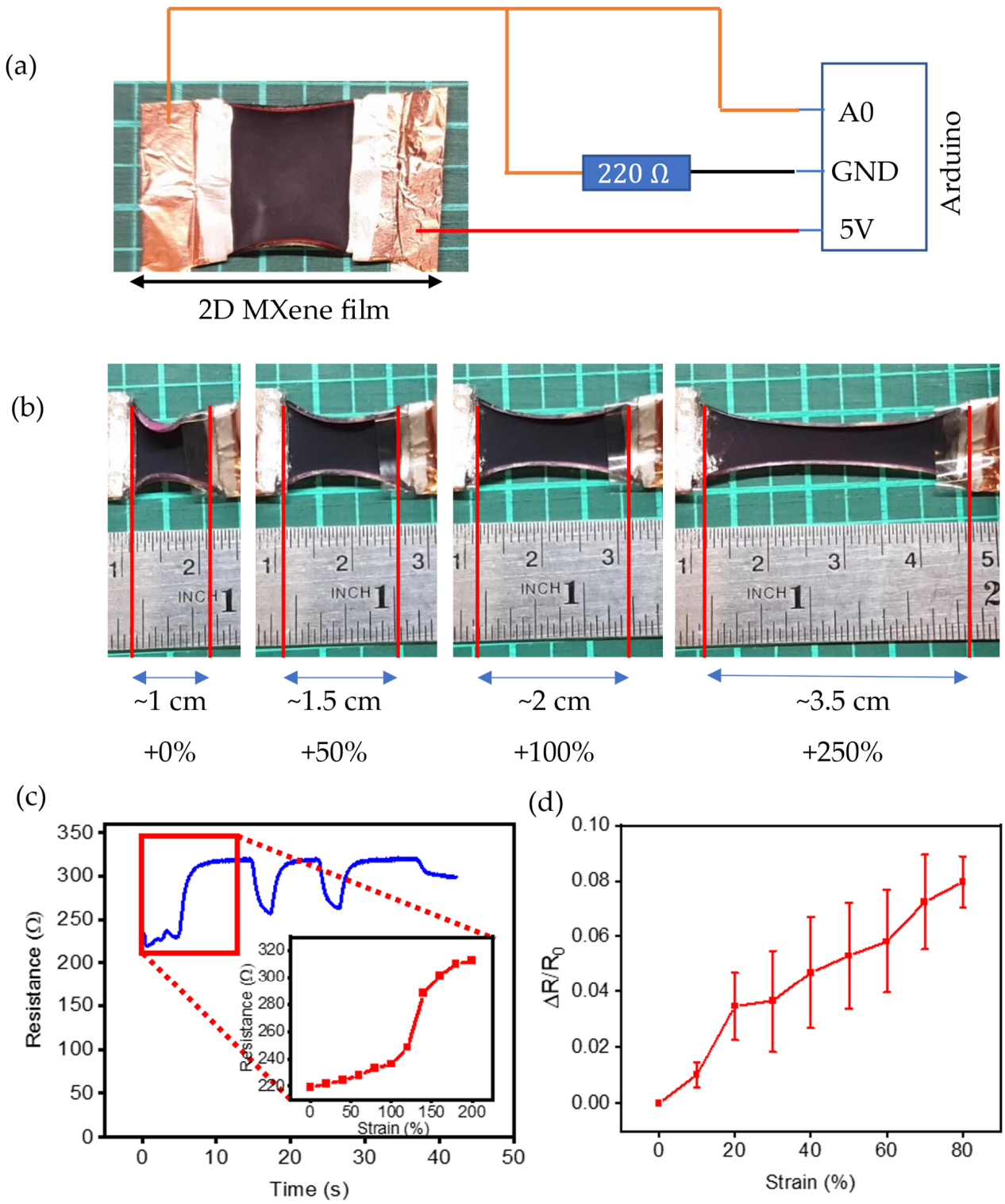

Figure 2. Characterization of the strain response of the wrinkled MXene strain sensor. (**a**) Circuit diagram using an Arduino for data collection. (**b**) Demonstration of the stretchability of the wrinkled MXene strain sensor under 0%, 50%, 100%, and 250% strain. (**c**) Graph of resistance values vs. time for a stretchable sensor. The inset shows the normalized resistance values compared to the strain percentage of the sensor. (**d**) The average strain response of the wrinkled MXene strain sensor up to 80% strain.

3. Results

3.1. Strain Response

To characterize the strain response, the wrinkled MXene strain sensor was slowly stretched and the change in resistance of the sensor was tracked over three cycles (Figure 2c). The initial resistance of the film was found to be around 220 Ω, and the strain sensor was observed to be able to withstand strain up to 250% (Figure 2b). The wrinkled MXene strain sensor was observed to have a significant strain response as the resistance value increased with strain. However, it plateaued at around 200% with a resistance value of about 320 Ω, with an approximate 25 Ω increase in resistance value under 50% strain. Even though the MXene strain sensor can be stretched up to 250%, the sensor became less responsive after each maximum strain, as seen by the upward drift in the baseline resistance in Figure 2c. With each cycle, upon releasing the sensor back to its original length, the baseline resistance of the sensor increased from 220 Ω to 230 Ω and eventually 260 Ω by the end of the third cycle. The response and recovery time of the sensor in response to strain were estimated to be roughly 500 ms and 170 ms, respectively.

The resistance values for the strain sensor are plotted against percentage strain (Figure 2c inset), where we observed a mostly constant increase in resistance values with increasing strain until ~80%. Between 80% and 120% strain, we observed a sharp increase in the resistance value, after which the resistance values plateaued, and the strain sensitivity of the sensor also decreased dramatically. Hence, while the sensor can be stretched to 250%, we took the effective strain limit of the sensor to be 80%. We measured and calculated the normalized change in resistance of the MXene strain sensor in response to strain within its effective strain limit. The sensitivity of the sensor is denoted by the gradient of the line in the normalized resistance value graph (Figure 2d), which is calculated to be ~0.1.

3.2. Pressure Response

We characterized the pressure response of the wrinkled MXene pressure sensor by measuring the change in resistance of the sensor in response to contact forces. We used 3 g weights in the form of 10 mm stainless steel hexagonal nuts (Figure 3a). To ensure even distribution of pressure on the wrinkled MXene pressure sensor, the weights were stacked on top of each other on a 10 × 10 mm rigid plastic square on the sensor itself. The pressure experienced by the sensor can be calculated using the following equation: $\text{Pressure} = \frac{\text{weight} * \text{gravitational acceleration}}{\text{Area}}$. In this case, each additional 3 g hexagonal nut corresponded to a pressure increase of 0.2943 kPa.

The pressure response of the wrinkled Mxene pressure sensor was charted onto a graph comparing the resistance response against time (Figure 3a) and a normalized resistance response against pressure (Figure 3c). To calculate the pressure sensitivity, we divided the pressure curve in Figure 3c into two regimes of interest (i) low-pressure regime (<0.25 kPa) and (ii) high-pressure regime (between 0.25 kPa and 2.0 kPa). We ignored the pressure response of the sensor beyond 2.0 kPa as the sensor's response was observed to have plateaued and was relatively unresponsive to further increases in pressure. We then best fitted the graph in each of the two regimes, with the gradient reflecting the pressure sensitivity.

There was a distinct resistance response whenever a load was placed and removed, which can be seen from the dips and spikes in resistance value (Figure 3a). An unstable response was observed during the initial loading phase, while the unloading phase showed more consistent results for the sensor characterization. Figure 3b shows the IV curves of the Mxene pressure sensor under various pressures, while Figure 3c shows the normalized resistance response of the pressure sensor during the unloading phase. We observed the sensitivity of the sensor to be 0.935 kPa^{-1} at the lower pressure regime (<0.25 kPa) and 0.188 kPa^{-1} at the higher-pressure regime (between 0.25 kPa and 2.0 kPa). The response and recovery time of the sensor in response to pressure were found to be roughly 250 ms and 400 ms, respectively.

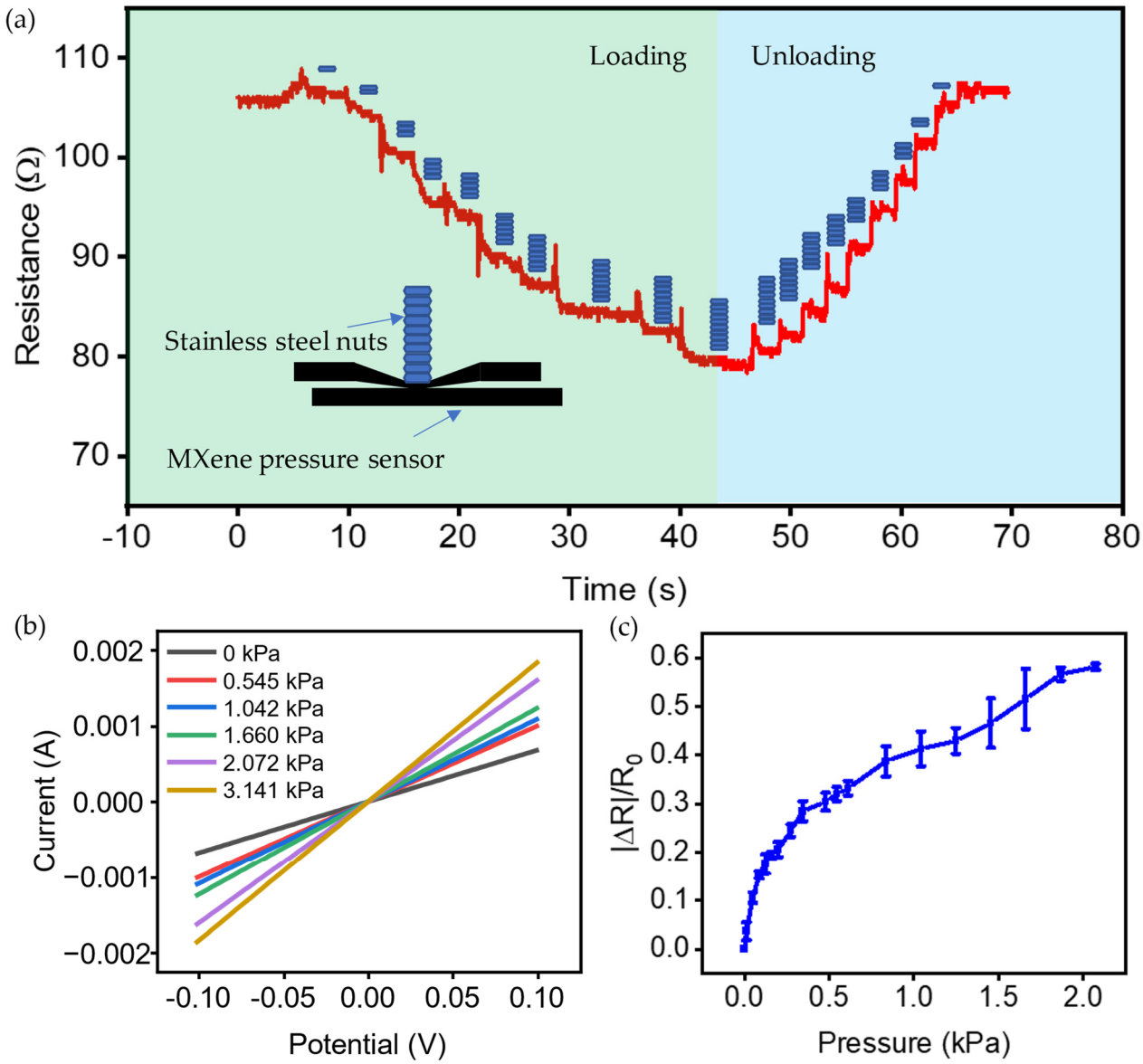

Figure 3. Characterization of the pressure response of the wrinkled MXene pressure sensor. (**a**) Resistance vs. time graph of the loading and unloading phase while adding 3 g steel nuts incrementally on the wrinkled MXene pressure sensor with the illustrated representation of the number of nuts on the sensor at the given time. (**b**) IV curves of the Mxene sensor under various pressures. (**c**) Normalized resistance vs. pressure graph of the unloading phase of the Mxene pressure sensor.

3.3. Vibration Frequency Response

To characterize the frequency response of the wrinkled Mxene pressure sensor, we attached a vibration motor to the Mxene sensor and the frequency was adjusted using the PWM output of the Arduino UNO microcontroller (Figure 4a). The vibration motor was powered 12 times and the vibration frequency was adjusted by supplying different amounts of power. We powered the vibration motor at 18,000 rpm and 9000 rpm to induce frequencies of 300 Hz and 150 Hz, respectively. The results were then processed through the Fast Fourier Transform (FFT) function in MATLAB to produce a single-sided Fourier transform graph of each of the above percentage powers. The sensor's response at both 150 Hz and 300 Hz can be seen in the Fourier transform (Figures 4b and 4c, respectively).

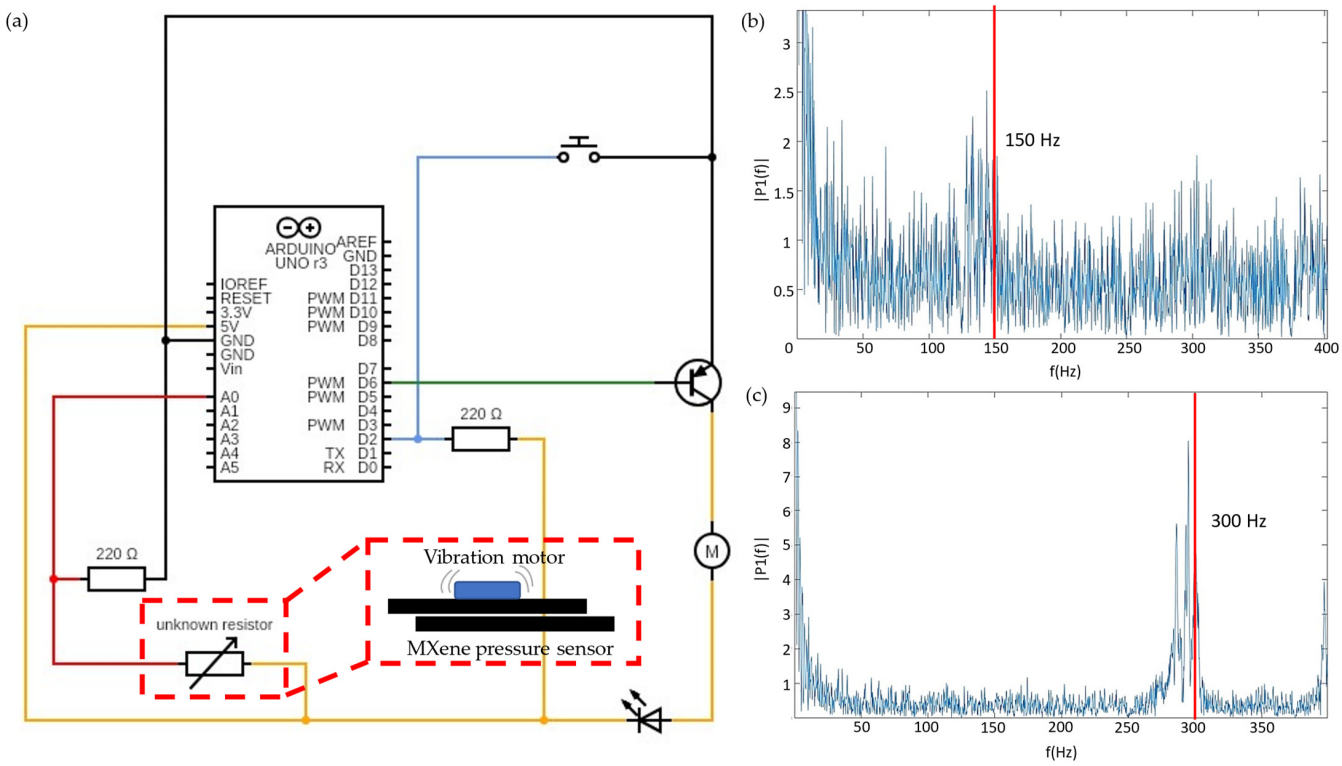

Figure 4. Characterization of the vibration frequency response of the wrinkled Mxene pressure sensor using a vibration motor. (**a**) Circuit schematic for measuring the dynamic frequency response of the sensor where a vibration motor is used to impose frequencies of 150 Hz (9000 rpm) and 300 Hz (180,000 rpm) on the sensor. (**b**) Fourier transformation of the sensor response via MATLAB FFT at 150 Hz and (**c**) 300 Hz, where the red lines denote the expected frequency output.

3.4. Mounting on Balloon

The work of Ref. [17] demonstrated that wrinkled actuators obtained from 3D buckling were compliant with reversible large curvatures due to the residual tensile strains that resulted from using curved pre-strained substrates. To explore whether 3D buckled wrinkled sensors have similar advantages in detecting changing curvatures, we attached a wrinkled Mxene pressure sensor to the surface of a commercial balloon and inflated the balloon to roughly twice its original size (200% strain). The electrodes of the sensor were connected to an Arduino setup to measure the changes in the resistance values of the sensor.

As the balloon expanded, the wrinkled Mxene pressure sensor also experienced a proportionate amount of strain, which corresponded to the increase in resistance values (Figure 5). The wrinkled Mxene pressure sensor showed the most response during the initial phases of inflation, as reflected by a steeper gradient in the resistance response. When the balloon was inflated to 200% of its original size, the strain sensor underwent roughly 50% strain. When comparing the normalized change in resistance values ($|\Delta R|/R_0$) of the sensor to the balloon's strain, we observed a more significant increase in resistance values in the lower strain regime (between 10% and 30% of strain). The resistance values then plateaued off and featured a relatively smaller change as it increased beyond 50% strain. The sensor demonstrated a decrease in strain sensitivity with increasing strain, implying that the sensor is more sensitive in the lower strain regimes. This may be partly due to the higher stiffness of the wrinkled Mxene sensor (as a result of the attached VHB substrate) as compared to that of the underlying balloon, where we observed that the expansion of the balloon was not able to generate sufficient force to stretch the sensor beyond 50%.

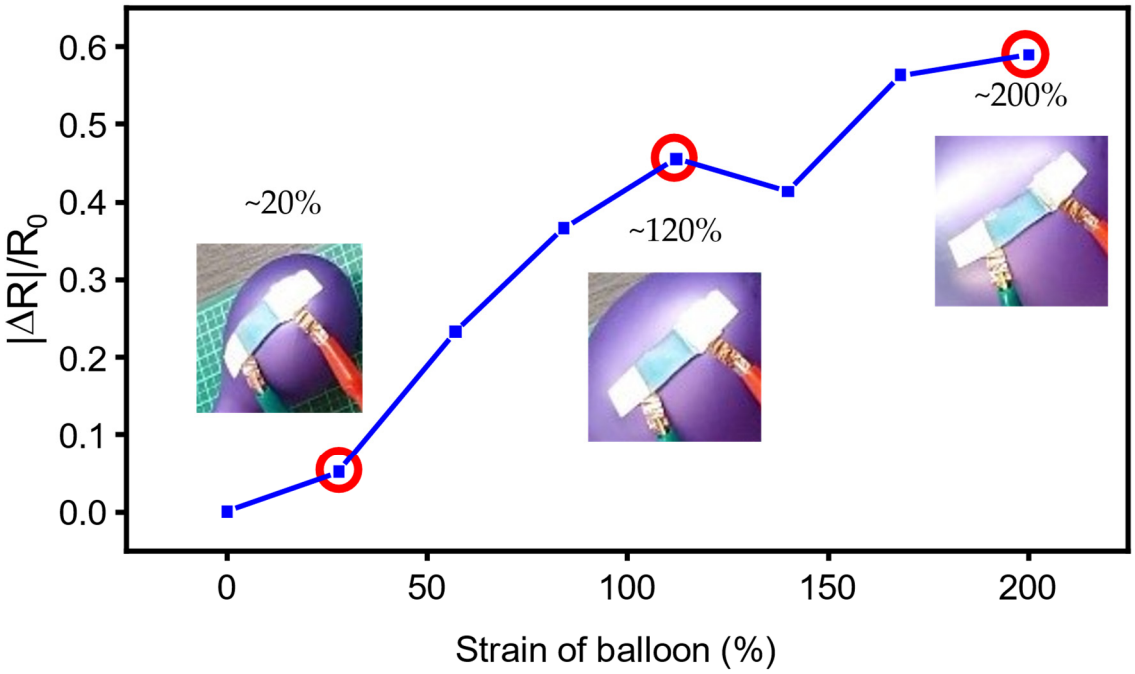

Figure 5. Characterization of the strain response of the Mxene pressure sensor in response to changing curvatures via inflation of a balloon.

4. Discussion

From Figure 2c, we observed that the wrinkled Mxene electrode was responsive to a strain of up to 80%. Due to the disordered orientation of the wrinkles obtained from 3D buckling, the peaks of the wrinkles often overlap and come into contact with each other. Unfolding these wrinkles will hence lead to a loss of contact between the wrinkle peaks, resulting in a rise in resistance, as reflected in the strain response of the sensor in Figure 2. The rapid increase in resistance followed by the plateau in sensor response beyond 80% strain could be attributed to various geometric factors contributed by the wrinkle morphology. The work of Ref. [19] observed similar behaviors in their 3D buckled wrinkled strain sensor and hypothesized that it could be due to a partial fracture in the wrinkled film. The shift in baseline resistance of the strain response of the MXene strain sensor in Figure 2c can be attributed to the hysteresis and inherent viscoelasticity of soft sensors [27]. In our work, we used normalized resistance values as this serves to correct for the baseline shift.

The resistance response of the wrinkled MXene pressure sensor displayed an unstable response during the initial loading phase of pressure, likely due to human error during the placement of the nuts on the sensor surface (Figure 3a). From Figure 3c, we observed the pressure sensor to be more sensitive in the lower pressure regime (<0.25 kPa). In pressure sensors based on contact resistance, the resistance changes of the sensor can be attributed to the change in contact resistance between both electrodes under pressure [2,8]. With increasing pressure, more wrinkle peaks of the two MXene electrodes come into contact with each other, resulting in a greater contact area and, consequently, lower contact resistance between the two electrodes [11]. The pressure sensor's response was observed to plateau beyond 2.0 kPa (Figure 3c). This was likely because the two MXene electrodes had fully contacted each other; hence, a further increase in pressure did not result in a decrease in contact resistance between the two MXene electrodes.

When comparing the MXene sensor capabilities to each other, namely strain and pressure sensing, the MXene pressure sensor exhibited more reliable and stable behavior. This may have been due to the fundamental difference in the structure of the sensors used

because the pressure sensor has a bilayer sensor structure while the strain sensor only has a monolayer structure.

Table 1 shows how the 3D buckled wrinkled MXene pressure sensor performs in comparison to past literature.

Table 1. Recent novel film-based pressure vibrotactile sensors and their characteristics compared to the wrinkled MXene pressure sensor tested in this paper for comparison.

Active Material	Working Mode	Working Range	Sensitivity	Response/Recovery Time	Frequency Tested at	Ref.
Ti3C2Tx-textile	Pressure	<5 kPa	19.78 kPa^{-1}	149 ms/139 ms	~3.3 Hz	[28]
MXene nanosheet	Pressure	10.2 Pa −30 kPa	2.52 kPa^{-1} (10–30 kPa)	11 ms/-	5 Hz	[29]
Paper-based SnSe2	Pressure	2–100 kPa	1.79 kPa^{-1}	100 ms/-	Finger tapping (~0.5 Hz)	[30]
Wrinkle-crumple reduced graphene oxide (rGO)	Pressure	0.5–4 kPa	0.055 kPa^{-1} (>50% strain)	100 ms/100 ms (>50% strain)	5 Hz	[2]
Patterned porous graphite	Pressure	<4 kPa	0.088 kPa^{-1}	100 ms/-	1 Hz −400 Hz	[31]
Human skin	Pressure	-	-	-	1–300 Hz	[6]
Wrinkled MXene	Pressure	0–2 kPa	0.935 kPa^{-1} 0.188 kPa^{-1}	250 ms/400 ms	25 Hz −300 Hz	This paper

The fabricated MXene sensors can potentially be used in various applications such as human motion detection [24,32] and sensors for soft robots and medical devices [2,32]. In their work, Ref. [33] found that when the sandwich structure fabrication method is employed such that the sensing materials are completely embedded and encapsulated in a flexible substrate, it can improve structural integrity and robustness, reduce buckling and possible fracturing of the sensing material, while minimizing unwanted deformation and wrinkling of the sensing material. Hence, in future work, we can encapsulate the sensor in elastomers (e.g., ecoflex, PDMS) to minimize oxidation of the wrinkled MXene film and ensure sensor stability.

Author Contributions: Conceptualization, H.R., P.-Y.C., D.Z.H.Y. and C.J.C.; methodology, D.Z.H.Y., C.J.C. and H.R.; validation, D.Z.H.Y. and C.J.C.; formal analysis, D.Z.H.Y. and C.J.C.; resources, P.-Y.C. and H.R.; writing—original draft preparation, D.Z.H.Y. and H.R.; writing—review and editing, C.J.C. and H.R.; supervision, P.-Y.C. and H.R. All authors have read and agreed to the published version of the manuscript.

Funding: This research was partly supported by the Key Project 2021B1515120035 of the Regional Joint Fund of the Basic and Applied Research Grant of Guangdong Province and Health Longevity Catalyst Awards 2022 (NAM & RGC Ref. No: HLCA/E-403/22).

Data Availability Statement: Not applicable.

Conflicts of Interest: The authors declare no conflict of interest.

References

1. Li, J.; Seng, Y.B.; Ponraj, G.; Kumar, K.S.; Cai, C.J.; Ren, H. Kirigami Strain Sensing on Balloon Catheters with Temporary Tattoo Paper. In Proceedings of the 2021 IEEE 17th International Conference on Wearable and Implantable Body Sensor Networks (BSN), Athens, Greece, 27–30 July 2021; IEEE: Washington, DC, USA, 2021; pp. 1–4.
2. Chang, T.H.; Tian, Y.; Li, C.; Gu, X.; Li, K.; Yang, H.; Sanghani, P.; Lim, C.M.; Ren, H.; Chen, P.Y. Stretchable Graphene Pressure Sensors with Shar-Pei-like Hierarchical Wrinkles for Collision-Aware Surgical Robotics. *ACS Appl. Mater. Interfaces* **2019**, *11*, 10226–10236. [CrossRef] [PubMed]
3. Dupont, P.E.; Simaan, N.; Choset, H.; Rucker, C. Continuum Robots for Medical Interventions. *Proc. IEEE* **2022**, *110*, 847–870. [CrossRef]
4. Kumar, K.S.; Zhang, L.; Kalairaj, M.S.; Banerjee, H.; Xiao, X.; Jiayi, C.C.; Huang, H.; Lim, C.M.; Ouyang, J.; Ren, H. Stretchable and Sensitive Silver Nanowire-Hydrogel Strain Sensors for Proprioceptive Actuation. *ACS Appl. Mater. Interfaces* **2021**, *13*, 37816–37829. [CrossRef] [PubMed]

5. Yang, J.; Ye, Y.; Li, X.; Lü, X.; Chen, R. Flexible, conductive, and highly pressure-sensitive graphene-polyimide foam for pressure sensor application. *Compos. Sci. Technol.* **2018**, *164*, 187–194. [CrossRef]
6. Liu, Y.; Pharr, M.; Salvatore, G.A. Lab-on-skin: A review of flexible and stretchable electronics for wearable health monitoring. *ACS Nano* **2017**, *11*, 9614–9635. [CrossRef] [PubMed]
7. Chortos, A.; Liu, J.; Bao, Z. Pursuing prosthetic electronic skin. *Nat. Mater.* **2016**, *15*, 937–950. [CrossRef] [PubMed]
8. Hammock, M.L.; Chortos, A.; Tee, B.C.K.; Tok, J.B.H.; Bao, Z. 25th anniversary article: The evolution of electronic skin (E-Skin): A brief history, design considerations, and recent progress. *Adv. Mater.* **2013**, *25*, 5997–6038. [CrossRef] [PubMed]
9. Zang, J.; Ryu, S.; Pugno, N.; Wang, Q.; Tu, Q.; Buehler, M.J.; Zhao, X. Multifunctionality and control of the crumpling and unfolding of large-area graphene. *Nat. Mater.* **2013**, *12*, 321–325. [CrossRef] [PubMed]
10. Wang, Q.; Zhao, X. Beyond wrinkles: Multimodal surface instabilities for multifunctional patterning. *MRS Bull.* **2016**, *41*, 115–122. [CrossRef]
11. Chen, W.; Gui, X.; Liang, B.; Yang, R.; Zheng, Y.; Zhao, C.; Li, X.; Zhu, H.; Tang, Z. Structural Engineering for High Sensitivity, Ultrathin Pressure Sensors Based on Wrinkled Graphene and Anodic Aluminum Oxide Membrane. *ACS Appl. Mater. Interfaces* **2017**, *9*, 24111–24117. [CrossRef] [PubMed]
12. Jung, W.B.; Cho, K.M.; Lee, W.-K.K.; Odom, T.W.; Jung, H.T. Universal method for creating hierarchical wrinkles on thin-film surfaces. *ACS Appl. Mater. Interfaces* **2018**, *10*, 1347–1355. [CrossRef] [PubMed]
13. Khang, D.; Rogers, J.A.; Lee, H.H. Mechanical buckling: Mechanics, metrology, and stretchable electronics. *Adv. Funct. Mater.* **2009**, *19*, 1526–1536. [CrossRef]
14. Chen, P.Y.; Sodhi, J.; Qiu, Y.; Valentin, T.M.; Steinberg, R.S.; Wang, Z.; Hurt, R.H.; Wong, I.Y. Multiscale Graphene Topographies Programmed by Sequential Mechanical Deformation. *Adv. Mater.* **2016**, *28*, 3564–3571. [CrossRef]
15. Chen, P.Y.; Liu, M.; Wang, Z.; Hurt, R.H.; Wong, I.Y. From Flatland to Spaceland: Higher Dimensional Patterning with Two-Dimensional Materials. *Adv. Mater.* **2017**, *29*, 1605096. [CrossRef] [PubMed]
16. Hu, X.; Dou, Y.; Li, J.; Liu, Z. Buckled Structures: Fabrication and Applications in Wearable Electronics. *Small* **2019**, *15*, 1804805. [CrossRef] [PubMed]
17. Tan, Y.; Chu, Z.; Jiang, Z.; Hu, T.; Li, G.; Song, J. Gyrification-Inspired Highly Convoluted Graphene Oxide Patterns for Ultralarge Deforming Actuators. *ACS Nano* **2017**, *11*, 6843–6852. [CrossRef] [PubMed]
18. Jing, L.; Xie, Q.; Li, H.; Li, K.; Yang, H.; Ng, P.L.P.; Li, S.; Li, Y.; Teo, E.H.T.; Wang, X.; et al. Multigenerational Crumpling of 2D Materials for Anticounterfeiting Patterns with Deep Learning Authentication. *Matter* **2020**, *3*, 2160–2180. [CrossRef]
19. Song, J.; Tan, Y.; Chu, Z.; Xiao, M.; Li, G.; Jiang, Z.; Wang, J.; Hu, T. Hierarchical Reduced Graphene Oxide Ridges for Stretchable, Wearable, and Washable Strain Sensors. *ACS Appl. Mater. Interfaces* **2019**, *11*, 1283–1293. [CrossRef]
20. Pang, J.; Mendes, R.G.; Bachmatiuk, A.; Zhao, L.; Ta, H.Q.; Gemming, T.; Liu, H.; Liu, Z.; Rummeli, M.H. Applications of 2D MXenes in energy conversion and storage systems. *Chem. Soc. Rev.* **2019**, *48*, 72–133. [CrossRef]
21. Ma, Y.; Liu, N.; Li, L.; Hu, X.; Zou, Z.; Wang, J.; Luo, S.; Gao, Y. A highly flexible and sensitive piezoresistive sensor based on MXene with greatly changed interlayer distances. *Nat. Commun.* **2017**, *8*, 1207. [CrossRef] [PubMed]
22. Li, H.; Du, Z. Preparation of a highly sensitive and stretchable strain sensor of MXene/silver nanocomposite-based yarn and wearable applications. *ACS Appl. Mater. Interfaces* **2019**, *11*, 45930–45938. [CrossRef] [PubMed]
23. Chang, T.H.; Zhang, T.; Yang, H.; Li, K.; Tian, Y.; Lee, J.Y.; Chen, P.Y. Controlled crumpling of two-dimensional titanium carbide (MXene) for highly stretchable, bendable, efficient supercapacitors. *ACS Nano* **2018**, *12*, 8048–8059. [CrossRef]
24. Cao, Y.; Guo, Y.; Chen, Z.; Yang, W.; Li, K.; He, X.; Li, J. Highly sensitive self-powered pressure and strain sensor based on crumpled MXene film for wireless human motion detection. *Nano Energy* **2022**, *92*, 106689. [CrossRef]
25. Tao, L.Q.; Zhang, K.N.; Tian, H.; Liu, Y.; Wang, D.Y.; Chen, Y.Q.; Yang, Y.; Ren, T.L. Graphene-Paper Pressure Sensor for Detecting Human Motions. *ACS Nano* **2017**, *11*, 8790–8795. [CrossRef]
26. Tian, H.; Shu, Y.; Wang, X.F.; Mohammad, M.A.; Bie, Z.; Xie, Q.Y.; Li, C.; Mi, W.T.; Yang, Y.; Ren, T.L. A graphene-based resistive pressure sensor with record-high sensitivity in a wide pressure range. *Sci. Rep.* **2015**, *5*, 8603. [CrossRef]
27. Yao, H.; Yang, W.; Cheng, W.; Tan, Y.J.; See, H.H.; Li, S.; Ali, H.P.A.; Lim, B.Z.H.; Liu, Z.; Tee, B.C.K. Near-hysteresis-free soft tactile electronic skins for wearables and reliable machine learning. *Proc. Natl. Acad. Sci. USA* **2020**, *117*, 25352–25359. [CrossRef]
28. An, J.; Ma, Y.; He, M.; Yan, J.; Zhang, C.; Li, X.; Shen, P.; Luo, S.; Gao, Y. A wearable and highly sensitive textile-based pressure sensor with Ti3C2Tx nanosheets. *Sens. Actuators A Phys.* **2020**, *311*, 112081. [CrossRef]
29. Guo, Y.; Zhong, M.; Fang, Z.; Wan, P.; Yu, G. A wearable transient pressure sensor made with MXene nanosheets for sensitive broad-range human–machine interfacing. *Nano Lett.* **2019**, *19*, 1143–1150. [CrossRef] [PubMed]
30. Tannarana, M.; Solanki, G.K.; Bhakhar, S.A.; Patel, K.D.; Pathak, V.M.; Pataniya, P.M. 2D-SnSe2 nanosheet functionalized piezo-resistive flexible sensor for pressure and human breath monitoring. *ACS Sustain. Chem. Eng.* **2020**, *8*, 7741–7749. [CrossRef]
31. Wu, Y.; Karakurt, I.; Beker, L.; Kubota, Y.; Xu, R.; Ho, K.Y.; Zhao, S.; Zhong, J.; Zhang, M.; Wang, X. Piezoresistive stretchable strain sensors with human machine interface demonstrations. *Sens. Actuators A Phys.* **2018**, *279*, 46–52. [CrossRef]
32. Yan, J.; Ma, Y.; Li, X.; Zhang, C.; Cao, M.; Chen, W.; Luo, S.; Zhu, M.; Gao, Y. Flexible and high-sensitivity piezoresistive sensor based on MXene composite with wrinkle structure. *Ceram. Int.* **2020**, *46*, 23592–23598. [CrossRef]
33. Yang, T.; Xie, D.; Li, Z.; Zhu, H. Recent advances in wearable tactile sensors: Materials, sensing mechanisms, and device performance. *Mater. Sci. Eng. R Rep.* **2017**, *115*, 1–37. [CrossRef]